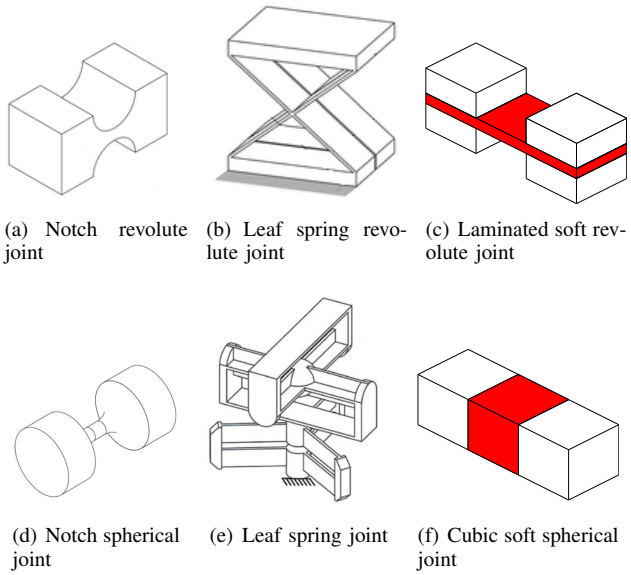
Kinematic Modeling of a Miniaturized Configurable Parallel Robot with Soft Joints for Real-Time Control

Maxence Leveziel, Guillaume J. Laurent, Michael Gauthier, Redwan Dahmouche*

***Abstract*—Reaching a high level of miniaturization and precision can be challenging when using classical mechanical joints. In contrast, soft joints can mimic the kinematic behavior of classical joints while enhancing precision by addressing issues like backlash. However, the accuracy of these joints heavily depends on their mathematical models, typically derived using Finite Element Models (FEM). Unfortunately, FEM models are time-consuming, which significantly complicates their implementation for real-time control. Consequently, the robot's positions must be pre-learned, restricting its ability to accurately reach new positions in real-time. In our study, we demonstrate that cubic soft joints can accurately mimic the kinematics of classical spherical joints, allowing for rapid computation of the robot's kinematic model. Comparisons with experimental results from a parallel miniature robot equipped with cubic soft joints and a configurable platform showed no significant difference between the proposed approximate model and more complex models like fine-meshed FEM. However, the simplified model operates thousands of times faster, which facilitates its implementation for real-time control. This breakthrough enables the modeling and design of complex miniaturized robot architectures, fostering new capabilities for dexterous manipulation at small scales.**



(a) Notch revolute joint (b) Leaf spring revolute joint (c) Laminated soft revolute joint

(d) Notch spherical joint (e) Leaf spring joint (f) Cubic soft spherical joint

Fig. 1. Examples of compliant joints (as represented in [7] and [8]) and their soft joint counterparts (the red parts represent soft materials).

I. Intruduction

The miniaturization of components, which makes devices smaller and more efficient, leads to the need to handle microcomponents for various tasks – manipulation and sorting of biological cells, microassembly of medical devices, etc. The various tasks are becoming increasingly complex and require greater dexterity, precision and speed. Specific robotic handling tools have been developed based on several micromanipulation principles [1], [2], [3]. Micromanipulation and microassembly operations typically require the use of micro-grippers or micro-tweezers. Currently, most of the micro tweezers are mounted on decimeter robotic manipulators [4], [5]. These solutions remain cumbersome, have a high inertia compared to the one of manipulated objects, and thus, reduce the overall performances, notably the manipulation speed. Reducing the size of the robot itself and its tools is a real need to gain in terms of performance and to significantly increase the manipulation efficiency [6].

The main obstacle to the miniaturization of mechanisms and, by extension, robots is closely related to the difficulties of miniaturizing mechanical joints. Indeed, usual mechanical joints such as revolute and spherical ones are not easily manufacturable at small scales. A common approach is to replace the standard joints with compliant ones, which can be obtained using local thinning of a single material or using two materials with different elastic moduli.

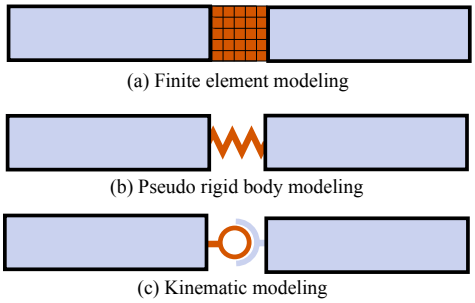
The local thinning solution uses the same material for the whole mechanism and thus is a monolithic part as shown in Fig. 1(a) and 1(d). Many geometries have been proposed with the main advantage being that the manufacturing of the mechanism does not require any assembly [7], [9]. The mechanical constraints are concentrated in a small region which is good for precision and accuracy but the deformations have to remain small to maintain the stresses below the elastic limit of the material. One way to obtain larger strokes is to switch from notches to continuous deformations along leaf springs as illustrated in Fig. 1(b) and 1(e) [7], [8], [10]. As a result, the stress is distributed along the beam and the joint allows much larger travel ranges. Nevertheless, the leaf springs are usually cumbersome which is incompatible with the miniaturization purpose.

The second solution to increase joint travel range is the use of soft joints. The compliant mechanism is obtained thanks to the difference in elastic moduli between the materials. In the literature, two main types of soft joints are distinguished for the realization of miniature robots. In the first one, the joints are manufactured with a laminating process [11] (see Fig. 1(c)). Many miniature robots are based on this principle

All Authors are with the FEMTO-ST Institute, Université de Franche-Comté, CNRS, SupMicroTech-ENSMM, Besançon, France.

This work was supported by the Grand Besançon Métropole, the French ANR project MiniSoRo (ANR-19-CE10-0004), and by EUR EIPHI program (ANR-17-EURE-0002). This work has been partly supported by the French ROBOTEX network (TIRREX ANR-21-ESRE-0015) and its FEMTO-ST technological facility CMNR. This work was carried out in part within the french RENATECH network and its FEMTO-ST technological facility MIMENTO.

*Corresponding author: redwan.dahmouche@femto-st.fr



(a) Finite element modeling

(b) Pseudo rigid body modeling

(c) Kinematic modeling

Fig. 2. Three types of models: the finite element model, the pseudo-rigid-body method, and the rigid-body method.

[12], [13], [14], [15]. This technique is more suitable for the realization of revolute joints. The design of spherical joints requires placing several hinges in series, which is cumbersome, reduces the joint travel range, and may induce undesirable gimbal locks. The second type of soft joints consists in printing or molding parts of elastomeric material into a rigid structure (see Fig. 1(f)). Using multi-material 3D printing or molding, it is possible to design joints with a wide variety of geometries allowing for the realization of miniature revolute or spherical-like joints [16], [17], [18], [19], [20], [21]. Indeed, the manufacturing of this type of joint using photolithography and molding has already been demonstrated [22], [23].

The modeling of the soft joints for miniature robots must fulfill several requirements. In particular, the computational time is a challenge for real-time control of miniature robots, where typical bandwidths can reach a hundred of hertz [12], [21]. As the deformation of soft joints relies on continuum mechanics, finite element modeling (FEM) can be used to accurately predict the deformations but its computational time may not be compatible with the real-time control loop of the robot. In our previous work, the robot's trajectory has been learned before its execution, which prevents the robot from adjusting its trajectory in real time if necessary or for performing tasks where the positions of the manipulated objects are not known in advance. Developing a fast and sufficiently accurate model would thus allow the use of external sensors (camera, etc.) to perform more complex tasks making the robot more versatile. Apart from FEM, the joint can also be represented by a pseudo-rigid-body model or even by a simple rigid-body model but the accuracy of these models may not be sufficient for the robot's operation. The choice of a model is therefore often a compromise between computation time and accuracy.

In this paper, we analyze different approaches to model of soft joints for miniature robots. We first review the three common methods that can be used to model mechanisms with soft joints, namely FEM, pseudo-rigid body models and classical rigid-body models. Then, we derive the rigid-body models of the MiGriBot, a parallel miniature robot with 18 soft joints and a configurable platform [21]. Finally, we compare the accuracy of the different models with experimental values.

II. Modeling of Soft Joints

A. Finite Element Model

The Finite Element Method (FEM) is the reference tool in the analysis of the deformation of continuum media. It consists of the division of the medium into several small sub-elements (mesh). Each element is modeled individually with linear or quadratic interpolation functions, and their interactions are combined to obtain the global deformations.

The design of most soft robots relies on FEM with commercial software like ABAQUS©, ANSYS©, or COMSOL© but also with academic ones like SOFA [24]. FEM can of course be used to model soft joints deforming inside a rigid structure as illustrated in Fig. 2(a). It can accurately predict the deformation of the soft joints subject to large deformations. However, the computational time and the memory space are high and directly linked to the number of elements in the mesh. The question that arises is to assess the added value of FEM in terms of accuracy compared with the computational time in the case of mechanisms with soft joints.

One of the simplifications that can be made is to consider 1D elements. In this case, a soft joint is described by one or more beam elements depending on its aspect ratio. If only one beam element is used per joint , the models become similar to the pseudo-rigid-body method.

B. Pseudo-Rigid-Body Model

The pseudo-rigid-body method is a lumped-parameter method that considers a flexible body as a collection of rigid bodies articulated by elastic discrete joints [25]. The degrees of freedom of the joints capture the deformation modes of the flexible unit. The springs and dampers capture their stiffness and damping characteristics. In the case of a soft joint, none of the degrees of freedom is blocked. The soft joint could be represented by torsional or/and translational springs that connect adjacent rigid links (Fig. 2(b)). The wrench and deformation of the joint are related by a generalized stiffness matrix K:

$$\begin{pmatrix} F \\ M \end{pmatrix} = K. \begin{pmatrix} D \\ \Theta \end{pmatrix} \tag{1}$$

The coefficient of the stiffness matrix is defined according to the geometry of the joint.

The pseudo-rigid-body method has been extensively used for compliant mechanisms. It has been also used to model soft joint mechanisms, for instance, the MilliDelta [12], the HSC joint [18], the leg mechanism [16] the miniature walking robot[17]. These works show that the pseudo-rigid-body models are accurate for small deformations and computationally efficient. The question is to know to what extent the pseudo-rigid-body method is suitable for mechanisms with soft joints subject to large deformations.

C. Rigid-body Model

The simplest solution is to consider the soft joints as an ideal spherical joint. This approach has been used with success to control the mini-RCM manipulator [13] and the portable

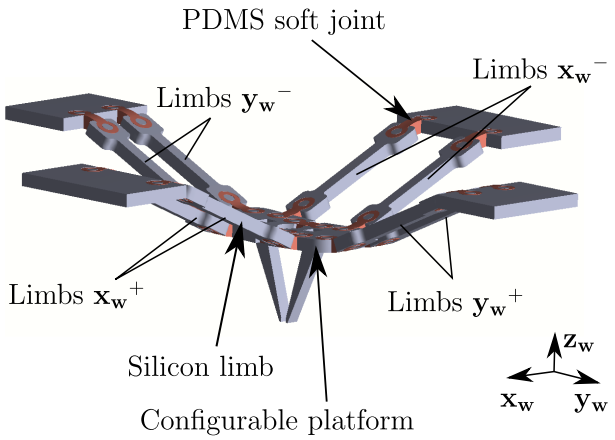


Fig. 3. The MiGriBot parallel mechanism with 18 soft joints [21].

haptic device [14] that are both based on revolute laminated soft joints.

The advantages of this approach are of course the simplicity of implementation and the use of all the tools used in robotics in a conventional way (direct and inverse modeling, singularity analysis, manipulability, etc.). Another important aspect is the short computational time. Conversely, this method is a coarse approximation of the real behavior of soft joints. The question is then to evaluate the loss of accuracy concerning the best FEM models.

III. Rigid-body Model

The considered robotic architecture illustrated in Fig. 3, is a parallel mechanism composed of 18 soft cubic joints (size ratio of 1) made of PDMS (polydimethylsiloxane) and 14 rigid links made of silicon [21]. Each part has a constant thickness of 0.4 mm and each silicon link has a length of 5 mm.

Figure 4 defines the geometrical parameters of the equivalent mechanism:

- u is the half-length of the platform in the $\mathbf{x_w}$ direction,
- w is the half-width of the platform in the $\mathbf{y_w}$ direction,
- v is the distance between the axis of the revolute joint and the line passing through the centers of the opposite spherical joints connected to actuators 1 and 3,
- l stands for the length of the limbs.

In order to derive the kinematic models of the MiGriBot, we define the following variables:

- $\mathbf{q} = (q_1, q_2, q_3, q_4)^{\mathrm{T}}$ is the configuration vector of the robot in the joint space where q_i is the linear position of the i$^{\text{th}}$ actuator (equals to the distance between origin O and point B_i),
- $\mathbf{x} = (x_p, y_p, z_p, \theta)^{\mathrm{T}}$ is the pose vector of the end-effector, where x_p, y_p z_p are the coordinates of the platform center point P, and θ is the angle between the right part of the platform and the horizontal plane.

Because of the symmetry of our architecture, only one variable (θ) is sufficient to define the opening/closing movement of the platform. Indeed, the angle between the left (respectively right) part and the horizontal is always the same because legs 1 and 3 are anchored at the same level to the platform. θ is then the half-opening angle of the gripper. When $\theta = 0$, the platform is flat.

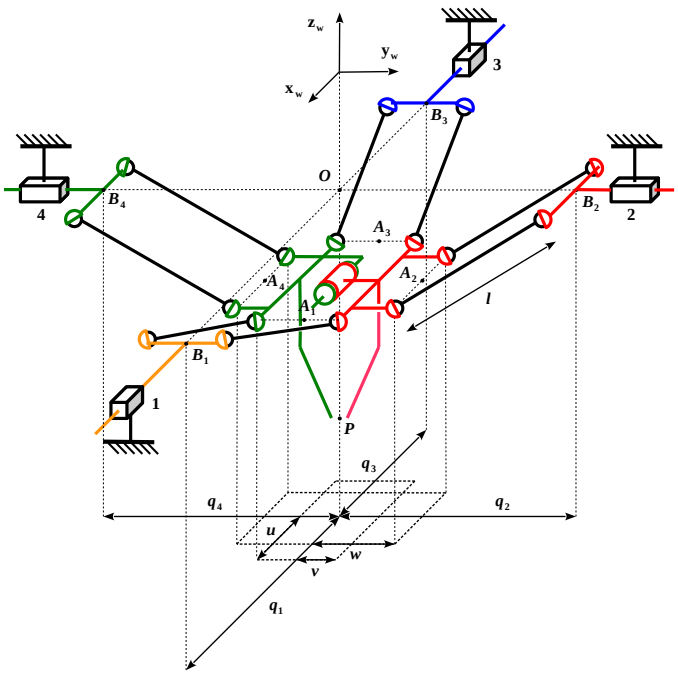


Fig. 4. Kinematic scheme of the MiGriBot, a 4-DoF parallel manipulator.

To keep constant the distance of the distal spherical joints of limbs 1 and 2 and then ensure the parallelism between the legs, the rotation between the right and left parts of the platform must be small. Indeed, the distance between these spherical joints is equal to $2v\cos(\theta)$ which can be approximated by its first-order Taylor expansion $2v + o(\theta^2)$. In practice, the flexibility of the legs and the joints compensate for the deviations of second order in the range of ten degrees at least.

A. Closure Equations

To write the closure equations, we express the coordinates of the points A_i and B_i in the world frame (see Fig. 4). Using the first-order Taylor expansion around zero for the cosine and sine functions, we get the following coordinates:

$$A_1 = \begin{pmatrix} x_p + u \\ y_p \\ z_p + v\theta \end{pmatrix}, \quad A_2 = \begin{pmatrix} x_p \\ y_p + w \\ z_p + w\theta \end{pmatrix}, \tag{2}$$

$$A_3 = \begin{pmatrix} x_p - u \\ y_p \\ z_p + v\theta \end{pmatrix}, \quad A_4 = \begin{pmatrix} x_p \\ y_p - w \\ z_p + w\theta \end{pmatrix}, \tag{3}$$

$$B_1 = \begin{pmatrix} q_1 \\ 0 \\ 0 \end{pmatrix}, \quad B_2 = \begin{pmatrix} 0 \\ q_2 \\ 0 \end{pmatrix}, \tag{4}$$

$$B_3 = \begin{pmatrix} q_3 \\ 0 \\ 0 \end{pmatrix}, \quad B_4 = \begin{pmatrix} 0 \\ q_4 \\ 0 \end{pmatrix}. \tag{5}$$

Then, the kinematic closure equations can be written:

$$\forall i \in \{1,2,3,4\}, \quad A_iB_i = \left\|\overrightarrow{A_iB_i}\right\| = l. \tag{6}$$

The expansions of the four squared equations are given by:

$$(x_p + u - q_1)^2 + {y_p}^2 + (z_p + v\theta)^2 = l^2, \tag{7}$$

$$(x_p - u - q_3)^2 + {y_p}^2 + (z_p + v\theta)^2 = l^2, \tag{8}$$

$${x_p}^2 + (y_p + w - q_2)^2 + (z_p + w\theta)^2 = l^2, \tag{9}$$

$${x_p}^2 + (y_p - w - q_4)^2 + (z_p + w\theta)^2 = l^2. \tag{10}$$

B. Inverse Kinematics Modeling

In the inverse kinematics problem, it is assumed that the end-effector position (x_p, y_p, z_p) and platform angle θ are known. The purpose is to find the joint positions (q_1, q_2, q_3, q_4).

Due to the presence of squared expressions, the development and separation of the different terms of the different closure equations lead to two possible configurations for each actuator q_i. The solutions of the inverse kinematics of the MiGriBot are then given by:

$$\begin{cases} q_1 = x_p + u + \varepsilon_1\sqrt{l^2 - {y_p}^2 - (z_p + v\theta)^2} \\ q_2 = y_p + w + \varepsilon_2\sqrt{l^2 - {x_p}^2 - (z_p + w\theta)^2} \\ q_3 = x_p - u - \varepsilon_3\sqrt{l^2 - {y_p}^2 - (z_p + v\theta)^2} \\ q_4 = y_p - w - \varepsilon_4\sqrt{l^2 - {x_p}^2 - (z_p + w\theta)^2} \end{cases} \tag{11}$$

with $\varepsilon_i \in \{1, -1\}$.

The assembly constraints allow us to choose the solutions for each actuator that are the farthest from the origin O, i.e. $\varepsilon_1 = \varepsilon_2 = \varepsilon_3 = \varepsilon_4 = 1$.

The closure equations give also a condition for a pose to be in the workspace. To be attainable, a pose $\mathbf{x} = (x_p; y_p; z_p; \theta)$ has to satisfy the following conditions:

$$\begin{cases} {y_p}^2 + (z_p + v\theta)^2 \leq l^2 \\ {x_p}^2 + (z_p + w\theta)^2 \leq l^2 \end{cases} \tag{12}$$

C. Forward Kinematics Modeling

In this section, we assume that joint positions (q_1, q_2, q_3, q_4) are known, and that the end-effector position (x_p, y_p, z_p) and platform angle θ should be determined. In order to find the analytical solution to the forward kinematics problem, we need to make linear combinations of the closure equations. The difference between Eq. (7) and (8) gives the value of x_p as a function of the actuators positions q_1 and q_3:

$$x_p = \frac{q_1 + q_3}{2} \quad \text{if} \quad q_1 - q_3 \neq 2u \tag{13}$$

The case where $q_1 - q_3 = 2u$ corresponds to the fact that the distance between the actuators q_1 and q_3 is the same as the length of the platform and, therefore, the limbs 1 and 3 are perpendicular to the platform. In other words, legs 1 and 3 are both vertical. In this case, x_p is not defined and the manipulator is in a singular configuration (see next section).

In a similar way considering Eq. (9) and (10), we obtain the expression for y_p as a function of the actuators positions q_2 and q_4:

$$y_p = \frac{q_2 + q_4}{2} \quad \text{if} \quad q_2 - q_4 \neq 2w \tag{14}$$

When $q_2 - q_4 = 2w$, the manipulator is also in a singular configuration (see next section).

To get the expressions of z_p and θ is less straightforward than for x_p and y_p. The first step is to get by linear combinations of the four closure equations, the two relations:

$$(7) + (8) \Rightarrow 2(z_p + v\theta)^2 = \underbrace{2l^2 - (x_p + u - q_1)^2 - (x_p - u - q_3)^2 - 2{y_p}^2}_{2a} \tag{15}$$

$$(9) + (10) \Rightarrow 2(z_p + w\theta)^2 = \underbrace{2l^2 - (y_p + w - q_2)^2 - (y - w - q_4)^2 - 2{x_p}^2}_{2b} \tag{16}$$

Then, the previous equations lead to four algebraic systems that correspond to the four possible assembly modes:

$$(S_1) \begin{cases} z_p + v\theta = \sqrt{a} \\ z_p + w\theta = \sqrt{b} \end{cases} \tag{17}$$

$$(S_2) \begin{cases} z_p + v\theta = -\sqrt{a} \\ z_p + w\theta = -\sqrt{b} \end{cases} \tag{18}$$

$$(S_3) \begin{cases} z_p + v\theta = \sqrt{a} \\ z_p + w\theta = -\sqrt{b} \end{cases} \tag{19}$$

$$(S_4) \begin{cases} z_p + v\theta = -\sqrt{a} \\ z_p + w\theta = \sqrt{b} \end{cases} \tag{20}$$

Among these four systems, (S_3) and (S_4) give an angle θ with values close to π which means that each side of the gripper would be flipped bottom to top. This assembly is not possible because it would requires to cross the legs.

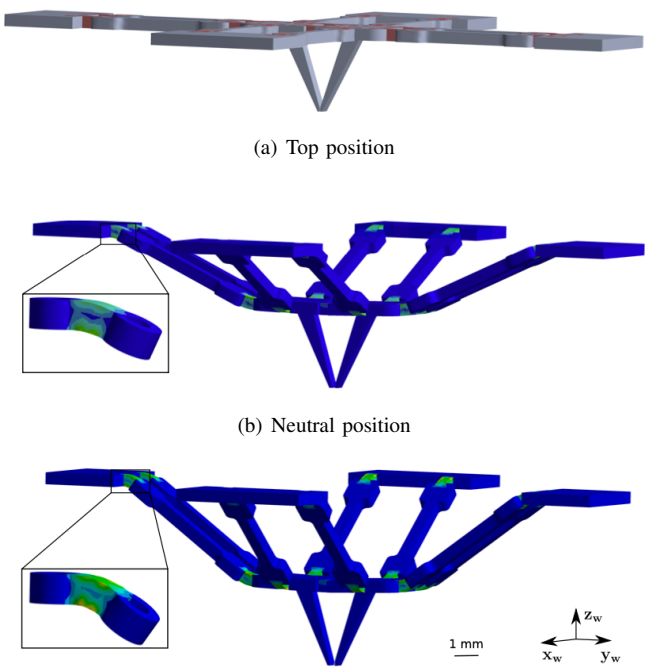
The systems (S_1) and (S_2) correspond to feasible solutions. Indeed, both give the same θ and z_p, but either both positive or negative. (S_1) corresponds to the assembly of the architecture above the plane $O\mathbf{x_w y_w}$, while (S_2) corresponds to the assembly of the architecture below.

To carry out the pick-and-place, the MiGribot must point downwards. So, the solution of the forward kinematics problem is chosen to be (S_2), and is given by:

$$\begin{cases} \theta &= \dfrac{\sqrt{a} - \sqrt{b}}{w - v} \\ z_p &= \dfrac{v\sqrt{b} - w\sqrt{a}}{w - v} \end{cases} \tag{21}$$

IV. Simulations and Experiments

To assess the accuracy of the proposed model ($C_{spherical}$), we compared it with two different models and with experimental results. The first model was obtained by considering the soft joints as 1D beam elements using the BeamAdapter



(a) Top position

(b) Neutral position

(c) Down position

Fig. 5. Stress inside the soft joints calculated by the reference A_{fine} model along a pure vertical trajectory (all the actuators receive the same inputs).

plugin of SOFA (S_{1D}). The stiffness matrix K of each beam element is given by:

$$\begin{pmatrix} \frac{AE}{L} & 0 & 0 & 0 & 0 & 0 \\ 0 & \frac{12EI_z}{L^3(1+\alpha_y)} & 0 & 0 & 0 & \frac{6EI_z}{L^2(1+\alpha_y)} \\ 0 & 0 & \frac{12EI_y}{L^3(1+\alpha_z)} & 0 & -\frac{6EI_y}{L^2(1+\alpha_z)} & 0 \\ 0 & 0 & 0 & \frac{GJ}{L} & 0 & 0 \\ 0 & 0 & -\frac{6EI_y}{L^2(1+\alpha_z)} & 0 & \frac{EI_y(4+\alpha_z)}{L(1+\alpha_z)} & 0 \\ 0 & \frac{6EI_z}{L^2(1+\alpha_y)} & 0 & 0 & 0 & \frac{EI_z(4+\alpha_y)}{L(1+\alpha_y)} \end{pmatrix} \quad (22)$$

with E the Young's modulus, G the shear modulus, $A = L^2$ the cross-sectional area, L the joint length, I_y and I_z the second moments of area, α_y and α_z the shear-deformation parameters.

The second model is obtained by FEM where the soft joints are discretized as 3D elements using ANSYS© (A_{fine}). Since the soft joints might be subject to large deformations, a nonlinear model with quadratic interpolations and regular 3D 40 µm tetrahedrons meshing were implemented. The silicon parts, considered as away more rigid then the soft joints, were modeled using 200 µm hexahedral meshing.

A. Simulation of a vertical trajectory

The four feet of the robot are moved toward the center position at the same distance making the platform go down as illustrated in Fig. 6. Looking at the vertical motion of the platform according to the actuator positions presented in Fig. 6, we can see that the positions predicted by the three tested models ($C_{spherical}$, S_{1D} and A_{fine}) are close to each other. The computational time goes from 0.9 ms for the rigid-body model $C_{spherical}$ to 6300 s for the 3D FEM model A_{fine}. The maximal position error between them is 7.6% for a travel range

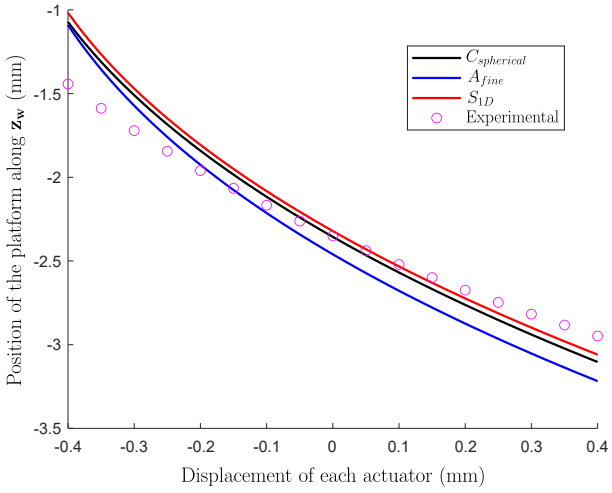


Fig. 6. Comparison between the experimental and the predicted positions by the $C_{spherical}$, S_{1D}, and A_{fine} models along a pure vertical trajectory (all the actuators receive the same inputs).

of 2.1 mm. The deviation can be explained by the fact that the A_{fine} model is more accurate (see Fig. 5) while compared to the two others.

Compared to the real experiments, the three models give an overestimation of z_w on the highest positions and an underestimation on the lowest positions. In other words, the movement of the real robot has a smaller amplitude than expected. The maximal position error is 16.0% at the highest position. This is most likely due to the assembly errors. However, in the central part of the workspace, where the robot is most used for pick-and-place operations, the different models are closer to the experimental measurements. Finally, one can notice that the beam and volume elements FEM models do not perform really better than the proposed model while being significantly slower. Using these more complex models while expecting better performances is thus not necessarily empirically justified.

B. Experimental validation of a pick-and-place trajectory

To analyze the accuracy of the proposed model while performing realistic tasks, we define a reference trajectory reported in black on Fig. 7 which consists of a U cycle with a constant opening of the gripper. The inverse kinematics of the rigid-body model $C_{spherical}$ was used to compute the four actuator inputs. These inputs were used for the experiments (circles correspond to the measured positions of the end-effector) and for all the models (lines are the prediction of the trajectory of the end-effector). Regarding the trajectory in the x_w, y_w plane (see Fig. 7), the three models ($C_{spherical}$, S_{1D} and A_{fine}) predict a very similar behavior. The maximal position error between the three models is 4.5% for a travel range of 0.2mm in height.

As for the vertical motion, all the models overestimate the z_w elevation. The maximal position error is 10.8% between the A_{fine} model and the experiments. These results confirm that the proposed spherical joint model represents a relevant compromise between the model accuracy and speed.

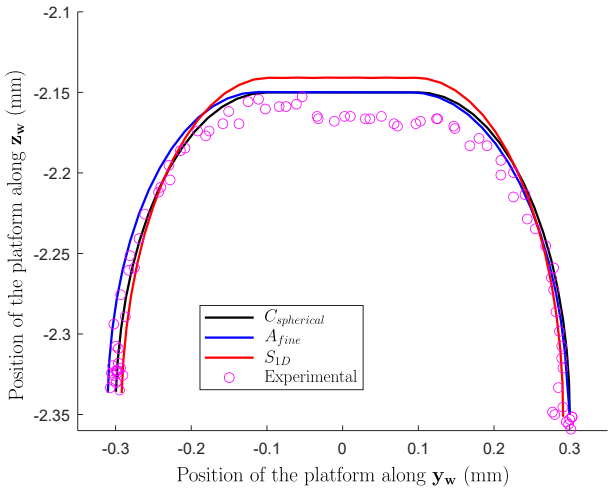


Fig. 7. Comparison between the experimental and the predicted positions by the $C_{spherical}$, S_{1D}, and A_{fine} models along a U-Shape trajectory in the $y_w; z_w$ plane.

V. Conclusion

In this paper, we have demonstrated that cubic soft joints can be used as spherical joints in miniaturized robots design. We have also shown that the models derived from this approximation are not significantly less accurate than FEM. In addition, the derived model can be computed at high speed (> 1 kHz on a standard PC), allowing for real-time implementation. This concept allows the design of miniaturized complex robotic architectures capable of unprecedented performance in terms of precision and speed. High throughput manipulation and sorting become conceivable with such a real-time model using MiGriBot, which has demonstrated 12 pick-and-place operations per second ($\times 10$ the state of art). In the future, the dynamic model will be derived using the same approach and compared with continuum mechanics methods to evaluate the limits of the proposed approach.

References

[1] M. Sitti, "Microscale and nanoscale robotics systems [grand challenges of robotics]," *IEEE Robotics & Automation Magazine*, vol. 14, no. 1, pp. 53–60, 2007.

[2] G.-Z. Yang, J. Bellingham, P. E. Dupont, P. Fischer, L. Floridi, R. Full, N. Jacobstein, V. Kumar, M. McNutt, R. Merrifield, *et al.*, "The grand challenges of science robotics," *Science robotics*, vol. 3, no. 14, p. eaar7650, 2018.

[3] M. Gauthier, P. Lambert, and S. Régnier, "Microhandling and micromanipulation strategies," *Microrobotics for micromanipulation*, pp. 179–242, 2013.

[4] D. Hériban and M. Gauthier, "Robotic micro-assembly of microparts using a piezogripper," in *2008 IEEE/RSJ international conference on intelligent robots and systems*, pp. 4042–4047, IEEE, 2008.

[5] Z. Lyu and Q. Xu, "Recent design and development of piezoelectric-actuated compliant microgrippers: A review," *Sensors and Actuators A: Physical*, vol. 331, p. 113002, 2021.

[6] R. Li and H. Qiao, "A survey of methods and strategies for high-precision robotic grasping and assembly tasks—some new trends," *IEEE/ASME Transactions on Mechatronics*, vol. 24, no. 6, pp. 2718–2732, 2019.

[7] D. Farhadi Machekposhti, N. Tolou, and J. Herder, "A review on compliant joints and rigid-body constant velocity universal joints toward the design of compliant homokinetic couplings," *Journal of Mechanical Design*, vol. 137, no. 3, p. 032301, 2015.

[8] J. Rommers, V. van der Wijk, and J. L. Herder, "A new type of spherical flexure joint based on tetrahedron elements," *Precision Engineering*, vol. 71, pp. 130–140, 2021.

[9] S. Linß, S. Henning, and L. Zentner, "Modeling and design of flexure hinge-based compliant mechanisms," in *Kinematics-Analysis and Applications*, IntechOpen, 2019.

[10] L. L. Howell, "Compliant mechanisms," in *21st century kinematics*, pp. 189–216, Springer, 2013.

[11] J. E. Correa, J. Toombs, N. Toombs, and P. M. Ferreira, "Laminated micro-machine: Design and fabrication of a flexure-based delta robot," *Journal of Manufacturing Processes*, vol. 24, pp. 370–375, 2016.

[12] H. McClintock, F. Z. Temel, N. Doshi, J.-s. Koh, and R. J. Wood, "The millidelta: A high-bandwidth, high-precision, millimeter-scale delta robot," *Science Robotics*, vol. 3, no. 14, 2018.

[13] H. Suzuki and R. J. Wood, "Origami-inspired miniature manipulator for teleoperated microsurgery," *Nature Machine Intelligence*, vol. 2, no. 8, pp. 437–446, 2020.

[14] S. Mintchev, M. Salerno, A. Cherpillod, S. Scaduto, and J. Paik, "A portable three-degrees-of-freedom force feedback origami robot for human–robot interactions," *Nature Machine Intelligence*, vol. 1, no. 12, pp. 584–593, 2019.

[15] M. Z. Miskin, A. J. Cortese, K. Dorsey, E. P. Esposito, M. F. Reynolds, Q. Liu, M. Cao, D. A. Muller, P. L. McEuen, and I. Cohen, "Electronically integrated, mass-manufactured, microscopic robots," *Nature*, vol. 584, no. 7822, pp. 557–561, 2020.

[16] D. E. Vogtmann, S. K. Gupta, and S. Bergbreiter, "Characterization and Modeling of Elastomeric Joints in Miniature Compliant Mechanisms," *Journal of Mechanisms and Robotics*, vol. 5, Oct. 2013.

[17] A. DeMario and J. Zhao, "Development and analysis of a three-dimensional printed miniature walking robot with soft joints and links," *Journal of Mechanisms and Robotics*, vol. 10, no. 4, 2018.

[18] A. Bruyas, F. Geiskopf, L. Meylheuc, and P. Renaud, "Combining multi-material rapid prototyping and pseudo-rigid body modeling for a new compliant mechanism," in *2014 IEEE International Conference on Robotics and Automation (ICRA)*, pp. 3390–3396, IEEE, 2014.

[19] R. S. Pierre, N. Paul, and S. Bergbreiter, "3dflex: A rapid prototyping approach for multi-material compliant mechanisms in millirobots," in *2017 IEEE International Conference on Robotics and Automation (ICRA)*, pp. 3068–3073, IEEE, 2017.

[20] C. Aygül, J. Kwiczak-Yiğitbaşi, B. Baytekin, and O. Özcan, "Joint design and fabrication for multi-material soft/hybrid robots," in *2019 2nd IEEE International Conference on Soft Robotics (RoboSoft)*, pp. 477–482, IEEE, 2019.

[21] M. Leveziel, W. Haouas, G. J. Laurent, M. Gauthier, and R. Dahmouche, "Migribot: A miniature parallel robot with integrated gripping for high-throughput micromanipulation," *Science Robotics*, vol. 7, no. 69, p. eabn4292, 2022.

[22] Z. Yang, B. Jeong, A. Vakakis, and S. Kim, "A tip-tilt-piston micromirror with an elastomeric universal joint fabricated via micromasonry," *Journal of Microelectromechanical Systems*, vol. 24, no. 2, pp. 262–264, 2015.

[23] W. Haouas, R. Dahmouche, J. Agnus, N. Le Fort-Piat, and G. J. Laurent, "New integrated silicon-pdms process for compliant micromechanisms," *Journal of Micromechanics and Microengineering*, vol. 27, no. 12, p. 127001, 2017.

[24] E. Coevoet, T. Morales Bieze, F. Largilliere, Z. Zhang, M. Thieffry, M. Sanz Lopez, B. Carrez, D. Marchal, O. Goury, J. Dequidt, and C. Duriez, "Software toolkit for modeling, simulation and control of soft robots," *Advanced Robotics*, vol. 31, pp. 1208–1224, Nov. 2017.

[25] V. K. Venkiteswaran and H.-J. Su, "A Three-Spring Pseudorigid-Body Model for Soft Joints With Significant Elongation Effects," *Journal of Mechanisms and Robotics*, vol. 8, 06 2016. 061001.